Active and widespread halogen chemistry in the tropical and subtropical free troposphere

Siyuan Wang[a,b,1], Johan A. Schmidt[c,d], Sunil Baidar[a,b], Sean Coburn[a,b], Barbara Dix[a], Theodore K. Koenig[a,b], Eric Apel[e], Dene Bowdalo[f], Teresa L. Campos[e], Ed Eloranta[g], Mathew J. Evans[f], Joshua P. DiGangi[h,2], Mark A. Zondlo[h], Ru-Shan Gao[i], Julie A. Haggerty[j], Samuel R. Hall[e], Rebecca S. Hornbrook[e], Daniel Jacob[c], Bruce Morley[j], Bradley Pierce[k], Mike Reeves[j], Pavel Romashkin[j], Arnout ter Schure[l], and Rainer Volkamer[a,b,3]

[a]Department of Chemistry & Biochemistry, University of Colorado, Boulder, CO 80309-0215; [b]Cooperative Institute for Research in Environmental Sciences, University of Colorado, Boulder, CO 80309-0216; [c]School of Engineering and Applied Sciences, Harvard University, Cambridge, MA 02138; [d]Department of Chemistry, University of Copenhagen, 2100 Copenhagen, Denmark; [e]Earth System Laboratory, Atmospheric Chemistry Division, National Center for Atmospheric Research, Boulder, CO 80307; [f]Department of Chemistry, University of York, York YO10 5DD, United Kingdom; [g]Space Science and Engineering Center, University of Wisconsin, Madison, WI 02138; [h]Department of Civil and Environmental Engineering, Princeton University, Princeton, NJ 08544; [i]Earth System Research Laboratory, Chemical Science Division, National Oceanic and Atmospheric Administration, Boulder, CO 80305; [j]Earth Observing Laboratory, Research Aviation Facility, National Center for Atmospheric Research, Boulder, CO 80307; [k]The National Environmental Satellite, Data, and Information Service, National Oceanic and Atmospheric Administration, Madison, WI 53706; and [l]Electric Power Research Institute, Palo Alto, CA 94304

Edited by Mark H. Thiemens, University of California, San Diego, La Jolla, CA, and approved June 9, 2015 (received for review March 13, 2015)

Halogens in the troposphere are increasingly recognized as playing an important role for atmospheric chemistry, and possibly climate. Bromine and iodine react catalytically to destroy ozone (O_3), oxidize mercury, and modify oxidative capacity that is relevant for the lifetime of greenhouse gases. Most of the tropospheric O_3 and methane (CH_4) loss occurs at tropical latitudes. Here we report simultaneous measurements of vertical profiles of bromine oxide (BrO) and iodine oxide (IO) in the tropical and subtropical free troposphere (10°N to 40°S), and show that these halogens are responsible for 34% of the column-integrated loss of tropospheric O_3. The observed BrO concentrations increase strongly with altitude (~3.4 pptv at 13.5 km), and are 2–4 times higher than predicted in the tropical free troposphere. BrO resembles model predictions more closely in stratospheric air. The largest model low bias is observed in the lower tropical transition layer (TTL) over the tropical eastern Pacific Ocean, and may reflect a missing inorganic bromine source supplying an additional 2.5–6.4 pptv total inorganic bromine (Br_y), or model overestimated Br_y wet scavenging. Our results highlight the importance of heterogeneous chemistry on ice clouds, and imply an additional Br_y source from the debromination of sea salt residue in the lower TTL. The observed levels of bromine oxidize mercury up to 3.5 times faster than models predict, possibly increasing mercury deposition to the ocean. The halogen-catalyzed loss of tropospheric O_3 needs to be considered when estimating past and future ozone radiative effects.

atmospheric chemistry | oxidative capacity | halogens | heterogeneous chemistry | UTLS

Tropospheric halogens catalytically destroy O_3 (1–3), oxidize atmospheric mercury (4, 5), and modify the oxidative capacity of the atmosphere (6). O_3 is a potent greenhouse gas (7), and an important precursor for hydroxyl (OH) radicals (6, 8) that determine the lifetime of CH_4 another important greenhouse gas. About 75% of the global tropospheric O_3 (3) and CH_4 (8) loss occurs at tropical latitudes, where O_3 radiative forcing is also most sensitive to changes in O_3 (9). Halogen chemistry is thought responsible for ~10% of the tropical tropospheric O_3 column loss (3), yet atmospheric models remain essentially untested due to the lack of vertically resolved halogen radical measurements in the tropical troposphere. Column observations from ground and satellites (10–18), including measurements in the tropics (14, 16–18), point to the existence of a—possibly ubiquitous—tropospheric BrO background concentration of ~1–2 parts per trillion by volume (pptv) that currently remains unexplained by models, and would be of significant relevance for O_3, OH, and mercury oxidation (2–6, 8). Recently, corroborating evidence is emerging from a measurement in the tropical free troposphere (FT) (19). IO has been detected in the Northern Hemisphere (NH) FT (19–21), but there is currently no vertically resolved measurement of BrO or IO in the Southern Hemisphere (SH) FT. The Eastern Pacific Ocean (EPO) is characteristic of the atmospheric preindustrial background (22), and is an area where the climate forcing is sensitive to changes in the tropospheric O_3 profile (9, 23).

Measurements

As part of the Tropical Ocean tRoposphere Exchange of Reactive halogen species and Oxygenated VOC (TORERO) field experiment (January/February 2012), we have measured tropospheric BrO and IO vertical profiles during a series of research flights (RFs) over the EPO. BrO and IO were detected in the open atmosphere by means of the University of Colorado Airborne Multi AXis Differential Optical Absorption Spectroscopy (CU AMAX-DOAS) instrument that measured scattered solar photon spectra in the limb geometry at different altitudes (19). Fig. 1 shows the unique specific

Significance

Our measurements show that tropospheric halogen chemistry has a larger capacity to destroy O_3 and oxidize atmospheric mercury than previously recognized. Halogen chemistry is currently missing in most global and climate models, and is effective at removing O_3 at altitudes where intercontinental O_3 transport occurs. It further helps explain the low O_3 levels in preindustrial times. Public health concerns arise from bioaccumulation of the neurotoxin mercury in fish. Our results emphasize that bromine chemistry in the free troposphere oxidizes mercury at a faster rate, and makes water-soluble mercury available for scavenging by thunderstorms. Naturally occurring bromine in air aloft illustrates global interconnectedness between energy choices affecting mercury emissions in developing nations and mercury deposition in, e.g., Nevada, or the southeastern United States.

Author contributions: R.V. designed research; S.B., B.D., E.A., T.L.C., E.E., M.A.Z., J.A.H., S.R.H., R.S.H., B.M., B.P., P.R., and R.V. performed research; S.W., J.A.S., S.C., B.D., T.K.K., D.B., M.J.E., D.J., B.P., and A.t.S. contributed new reagents/analytic tools; S.W., J.A.S., S.B., S.C., B.D., T.K.K., E.A., T.L.C., E.E., J.P.D., M.A.Z., R.-S.G., J.A.H., S.R.H., R.S.H., B.M., B.P., M.R., P.R., and R.V. analyzed data; and S.W., J.A.S., and R.V. wrote the paper.

The authors declare no conflict of interest.

This article is a PNAS Direct Submission.

Freely available online through the PNAS open access option.

[1]Present address: Department of Chemistry, The Hong Kong University of Science and Technology, Hong Kong, China.

[2]Present address: Langley Research Center, National Aeronautics and Space Administration, Hampton, VA 23681.

[3]To whom correspondence should be addressed. Email: rainer.volkamer@colorado.edu.

This article contains supporting information online at www.pnas.org/lookup/suppl/doi:10.1073/pnas.1505142112/-/DCSupplemental.

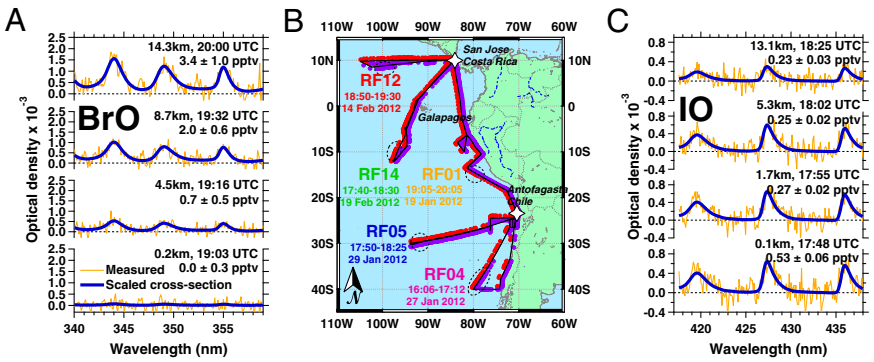

Fig. 1. Spectral proof of the detection of (*A*) BrO, RF01 in the tropical FT, and (*C*) IO, RF05 in the SH subtropical FT; red dots in (*B*) map of study area indicate locations along the flight tracks where BrO was detected above detection limit, while blue dots represents those for IO. AMAX-DOAS detection limits are ∼0.3–0.6 pptv for BrO and ∼0.04–0.1 pptv for IO (19) (see *Methods*). Dashed circles on *B* refer to the profiling locations. The unique BrO and IO fingerprint absorptions are shown in optical density units (the product of absorption cross-section times slant column density; it is overlaid on top of the instrument noise) for spectra of scattered solar photons collected during limb viewing forward of the aircraft at various altitudes.

absorption bands of BrO and IO, appropriately scaled and overlaid on the noise level of the instrument. These spectra provide unambiguous "spectral proof" for the presence of both radicals in the tropical FT, and their changing abundance with altitude. Also shown is a spectrum recorded at an altitude of 0.1 km that shows BrO below the detection limit (here ∼0.5 pptv; see *Methods*). Fig. 1*B* shows that BrO and IO were frequently above the detection limit in the FT, and are widespread between 10°N and 40°S latitude. That BrO and IO are detected consistently in both hemispheres at tropical latitudes in our study area calls for vertically resolved measurements in other longitude sectors, and different seasons.

Fig. 2 shows the BrO vertical profiles during five RFs in tropical (RF01, RF12, RF14), and SH subtropical air (RF04, RF05). BrO was consistently detected above 2–4 km, and generally BrO mixing ratios increased with altitude. These flights were selected for cloud-free conditions, and lack of obvious pollution influences in the upper FT (above 6–8 km), as confirmed by analyses of back-trajectories and tracer measurements made on the aircraft (*SI Appendix*, Figs. S2 and S3). In the lower FT, elevated CO (> 60 parts per billion by volume (ppbv); *SI Appendix*, Fig. S2) is attributed to pollution outflow from South America and influence from biomass burning. In the tropics, RF01, RF12, and RF14 mostly probed aged FT air with minor influences from aged (3–7 d) marine deep convection. No evidence was found for stratospheric influence during RF01, RF12, and RF14 over at least 7 d, from the surface up to ∼14 km (see *SI Appendix*, Fig. S3). By contrast, RF04 and RF05 experienced recent stratospheric influences (*SI Appendix*, Fig. S4) in the form of stratospheric intrusion (RF04, $O_{3,max}$ = 135 ppbv at 11 km, decreasing O_3 and BrO above 12 km) and a double tropopause (RF05, above 11 km). The consistency between four of the five profiles, probed 31 d apart (RF01 vs. RF14) and separated by a horizontal distance of ∼5,000 km, is remarkable. Under double-tropopause conditions, we observed BrO (13 km: RF05, 4.0 ± 0.5 pptv) that was slightly higher than in the tropical upper troposphere (13 km: RF01, 3.4 ± 1.0 pptv; RF12, 3.0 ± 0.7 pptv; RF14, 3.5 ± 0.6 pptv), and a steepening increase was observed above 12 km (RF01, RF05, RF14); at SH midlatitudes, BrO decreased above 12 km (13 km: RF04, 1.1 ± 0.4 pptv). Previous attempts to measure vertical profiles of tropospheric BrO used direct sun observations (24, 25) and yielded about an order of magnitude lower BrO than ground-based and satellite measurements (11–18), which observed tropospheric BrO vertical column densities (VCD) of 1–3 × 10^{13} molecules per square centimeter (molec × cm^{-2}). Our limb-viewing profile integrals range from 1.0 × 10^{13} (RF04) to 1.7 × 10^{13} (RF05)

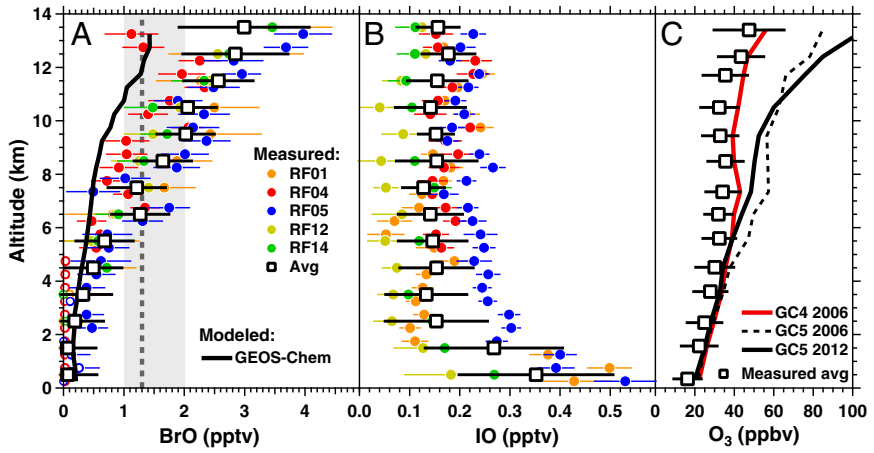

Fig. 2. Vertical profiles of (*A*) BrO, (*B*) IO, and (*C*) O_3 during RF01, RF04, RF05, RF12, and RF14. AMAX-DOAS measured BrO and IO are shown as solid circles, while the campaign-averaged profiles of BrO, IO, and O_3 are shown as open boxes. Solid black line in *A* is the campaign average GEOS-Chem (Goddard Earth Observation System - Chemistry model) base case simulation (GEOS-5 meteorological field). Also shown in *A* is the tropospheric BrO background in the tropical latitudes inferred from satellite (gray shading) and the equivalent tropospheric BrO level calculated using AMAX-DOAS data in this work (dashed gray vertical line). *C* shows campaign averages of GEOS-Chem modeled O_3 using GEOS-4 and GEOS-5 inputs.

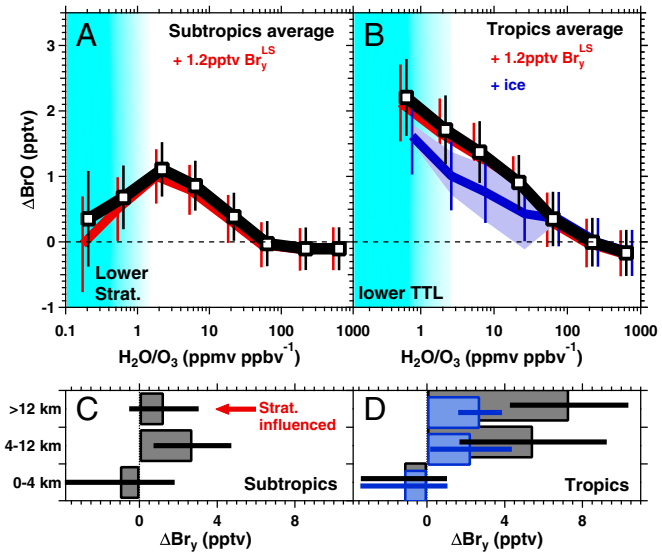

Fig. 3. ΔBrO vs. H_2O/O_3 in subtropical (*A*) and tropical (*B*) latitudes, as well as vertically binned ΔBr_y in the subtropics (*C*) and tropics (*D*). ΔBrO is defined as the BrO difference between AMAX-DOAS measured and BM calculated, while ΔBr_y is defined as the difference between Br_y inferred from AMAX-DOAS measurements and BM modeled. Black represents GEOS-Chem Br_y redistributed by BM, while blue (in *B* and *D*) denotes BM calculations including ice heterogeneous chemistry (ice content calculated by GEOS-5). Blue shading (*B*) shows sensitivity runs with ice content multiplied by ~0.1–10. Error bars in *A* and *B* are ΔBrO uncertainty propagated from both measurement uncertainty, ~30% modeling uncertainty and atmospheric variability (among different RFs), while error bars in *C* and *D* are ΔBr_y uncertainty propagated from ΔBrO uncertainty. Cyan shadings (*A* and *B*) show rough regimes corresponding to lower stratosphere (Strat.) or lower TTL.

molec × cm^{-2} BrO VCD, with a tropical average of 1.5×10^{13} molec × cm^{-2} (RF01, RF12, RF14). This is 12% lower than the VCD equivalent to 1 pptv BrO throughout the troposphere (14) (corresponds to 1.7×10^{13} molec × cm^{-2} below 13 km), and closely resembles the January/February average BrO VCD measured by the GOME-2 (Global Ozone Monitoring Experiment-2) satellite (~1.6×10^{13} molec × cm^{-2}, 30°N–30°S) (18). The good agreement with satellites may be coincidental, since the satellite averages globally over tropical longitudes. However, it supports the widespread relevance of our findings. There have been no previous measurements that detected tropospheric BrO in the SH tropics or subtropics. Our measurements are consistent with recent evidence from the NH tropical FT (19) and support the assertion that BrO is ubiquitous in the global FT (see *SI Appendix*) (16–19). The vertical profiles provide missing a priori information for improved interpretations of satellite and ground-based observations.

Our IO measurements extend the altitude range over which IO has been measured from aircraft, and present, to our knowledge, the first IO profiles in the SH subtropics. In the marine boundary layer (MBL), IO varied between ~0.18 pptv and 0.54 pptv and decreased with altitude (Fig. 2*B*). In the lower FT, continental air (RF01) contained less IO than air influenced by marine deep convection (RF05), which is consistent with a marine source of precursors. The elevated IO in the transition layer (~1.5 km altitude) corroborates previous evidence (20, 21), and is inconsistent with the IO lifetime limited by irreversible iodine loss to aerosol surfaces (20). Dix et al. (20) speculated that heterogeneous reactions on aerosol surfaces might recycle IO (20), possibly by releasing I_2, and HOI (26). This hypothesis deserves further investigation in light of widespread elevated IO observed in this study. The IO VCD in the SH tropics (RF01: 3.5×10^{12} molec × cm^{-2}; RF14: 2.6×10^{12} molec × cm^{-2}) and SH subtropics (RF05: 5.1×10^{12} molec × cm^{-2}) compares to 2.3×10^{12} molec × cm^{-2} over the NH tropical EPO (tEPO) (19) and ~1×10^{12} molec × cm^{-2} over the NH tropical Central Pacific Ocean (tCPO) (20). Notably, IO was about 2–3 times higher during all case studies in the SH FT. The IO profile shape in the SH is generally consistent with previous observations in the NH (19). We found no indication for lower IO under stratospheric influences (RF04, RF05).

Model Comparisons

Atmospheric models underestimate BrO in the tropical FT. The first tropospheric bromine chemistry model study was by von Glasow et al. (2), who predicted a tropical tropospheric BrO column of $<0.5 \times 10^{13}$ molec × cm^{-2}. Yang et al. (27) parameterized sea salt debromination in the global chemical transport model p-TOMCAT (Tropospheric Off-line Model of Chemistry and Transport), based on Sander et al. (28), and predicted tropical tropospheric BrO column of $<0.4 \times 10^{13}$ molec × cm^{-2}. Different global chemistry transport models, such as GEOS-Chem (6), CAM-Chem (Community Atmosphere Model with Chemistry) (3, 29), and Modal-CAM (30), represent tropospheric bromine chemistry quite differently, but consistently predict tropospheric BrO columns below 1×10^{13} molec × cm^{-2} in the tropics. The measured BrO VCD is 2–4 times higher than the tropospheric BrO VCD predicted by GEOS-Chem (6) (Fig. 2), which predicts average BrO VCD of 0.62×10^{13} molec × cm^{-2} in the tropics (0.76, 0.66, and 0.45×10^{13} for RF01, RF12, and RF14, respectively), and 0.94×10^{13} molec × cm^{-2} in the SH subtropics (0.77 and 1.1×10^{13} molec × cm^{-2} for RF04 and RF05, respectively). The horizontal distribution of BrO and Br_y (defined as Br + BrO + HBr + HOBr + $BrONO_2$ + $BrNO_2$ + 2*Br_2) in the model shows significant variability due to a Br_y "hole" over the Amazon rain forest (*SI Appendix*, Fig. S5). To account for atmospheric variability in the TORERO study area, the model is compared with the average measurements of tropical and subtropical profiles, and not with individual profile case studies. Model predictions find considerably lower BrO than surrounding areas over east Brazil, where previous balloon-borne profiles near Teresina had found lower upper limits (<1–2 pptv) (24, 25) for tropospheric BrO (see *SI Appendix*). The difference from previous balloon profiles most likely reflects atmospheric variability, i.e., the lack of ocean sources of organohalogen source gases and sea salt over land, and efficient tropospheric Br_y washed out by deep convection over the Amazon. By contrast, the TORERO study area is downwind of convection over oceans. Over the tEPO, the difference between measured and box model (BM) predicted BrO (BM constrained by GEOS-Chem Br_y and measurements of photolysis frequencies, O_3, NO_2, CO, CH_4, aerosol size distributions, etc.; see *SI Appendix* for details), ΔBrO, shows a strong relationship with air mass history (Fig. 3). The largest ΔBrO (~2.2 pptv) is observed in the lower tropical transition layer (TTL). In the tropics, ΔBrO strongly correlates with H_2O/O_3 tracer ratios ($R^2 = 0.99$, Fig. 3*B*), and is highest in dry air that has spent at least 3–7 d (possibly much longer) in the upper FT (*SI Appendix*, Fig. S3). In the SH subtropics, a similar trend for increasing ΔBrO is observed in the mid FT. However, ΔBrO decreases in the lower stratosphere (LS; Fig. 3*A*), consistent with previous observations (31), but remains slightly positive. The measured BrO corresponds to between 4.6 pptv and 8.2 pptv Br_y in LS air. Frequent intrusions of extratropical LS air into the tropical upper troposphere have been observed near 120°W and 30°W (32, 33), including—but not limited to—the region upwind of our study area. To test the influence of persistent extratropical LS forcing (32, 33), a set of model simulations were performed that varied the LS Br_y burden in GEOS-Chem to gauge the sensitivity of BrO. The average ΔBrO in LS air was ~0.5 pptv, and corresponds to ~1.2 pptv additional LS Br_y (compare Fig. 3*C*). If added to the LS Br_y burden, a slight increase in BrO is observed above 10 km in the subtropics (*SI Appendix*, Fig. S6 *F* and *G*), but tropical BrO remains essentially unchanged at all altitudes (*SI Appendix*, Fig. S6 *A* and *B*). We conclude that the amount of Br_y in the LS deserves further study, but that stratospheric influences alone

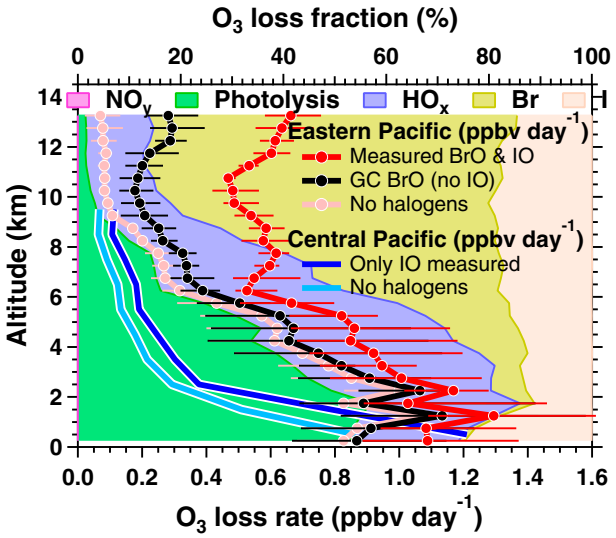

Fig. 4. Ozone loss rate and percentage contribution as calculated by box model. The box model was constrained to the median measured BrO and IO profiles using data from RF01, RF05, RF12, and RF14; profiles in Central Pacific are reproduced from Dix et al. (20) (only IO was measured; BrO is assumed to be ~0.5 pptv for lack of measurements here). Error bars show 25th/75th percentiles among the five RFs to represent the atmospheric variability.

are unlikely to explain the elevated BrO in the tropical TTL, and in the tropical and subtropical mid FT.

Tropospheric Bromine Sources

Oceanic emissions of $CHBr_3$ and CH_2Br_2 were measured aboard the aircraft, and are found to be in reasonable agreement with GEOS-Chem predictions (*SI Appendix*, Fig. S6). The GEOS-Chem Br_y production rate above 10 km, from $CHBr_3$, CH_2Br_2, and CH_3Br, accounts for 97% of the production from box model calculations constrained by Trace Organic Gas Analyzer (TOGA) measured organohalogen species ($CHBr_3$, CH_2Br_2, CH_2BrCl, $CHBr_2Cl$) and GEOS-Chem predicted CH_3Br. The additional contributions of halons (other than CH_3Br) to Br_y is estimated using tropospheric lifetimes as compiled in the *WMO Scientific Assessment of Ozone Depletion: 2014* (34), and accounts for < 0.1% additional tropospheric Br_y production. These estimates support that the uncertainty due to emissions of $CHBr_3$, CH_2Br_2, or missing organohalogens in GEOS-Chem have a very small effect on the tropospheric Br_y production rate. We conclude that the uncertainty regarding organohalogens is insufficient to explain the elevated BrO measurements. Heterogeneous reactions are known to play an important role in determining the chemical transformation of inorganic Br_y species. Recent studies highlight the importance of Br_y recycling on ice crystals (35) and the corresponding impacts on the partitioning and the washout efficiency of Br_y in the TTL (29). Heterogeneous reactions of O_3 with particulate bromide (36–38), or recycling of HOBr and HBr on ice crystals, increase the BrO/Br_y ratio (*SI Appendix*, Fig. S6) and the Br_y burden. The latter is because HBr and HOBr are highly water soluble, while Br_2 and BrO are only slightly soluble (Henry's law constant at 298 K moles per liter per atmosphere (6): HBr: 7.5×10^{13} (effective); HOBr: 6100; Br_2: 0.76; BrO: 0.71). Cirrus clouds are widespread in the TTL over the tEPO (39). Our airborne High Spectral Resolution Lidar (HSRL) observations detected ice crystals above 7 km altitude during RF12 and RF14 (*SI Appendix*, Fig. S7). We have constrained a box model with observations (see *Methods*) and find that heterogeneous recycling on ice crystals (ice surface area taken from GEOS-5; see *SI Appendix*, Fig. S6*E*) greatly reduces the model–measurement discrepancy in the tropical FT. The ΔBrO error bars in Fig. 3 *A* and *B* reflect measurement and modeling uncertainties (~0.3 pptv BrO and ~30% model, respectively), and further consider atmospheric variability among different RFs. As seen, ΔBrO is compatible with zero below 11 km for the ice recycling model run (Fig. 3*B*; see also *SI Appendix*, Fig. S6). However, ΔBrO remains significant and positive in the lower TTL (Fig. 3*B*). This suggests that additional Br_y is needed, which likely originates from an additional source, but we cannot rule out the possibility that Br_y deposition is less efficient than suggested by the model. Our best estimate points to ~2.5–6.4 pptv equivalent Br_y (Fig. 3), which is unlikely to be of organic or stratospheric origins.

Sea salt debromination is known be an important source of Br_y (6, 27, 29, 30), and generally assumed to be confined to the MBL due to efficient wet removal of sea salt aerosol. Global models find that, depending on size, sea salt aerosol lifetimes vary from minutes to days (6, 29), and the vertical distribution is skewed heavily toward the lowest 1–2 km. However, sea salt signatures have been observed in anvil cirrus encounters at ~12–14 km in the tropical and subtropical latitudes, including flights over the tEPO (40, 41). Froyd et al. (40) analyzed anvil cirrus residue collected from 12 km to 14 km over the tEPO and found >50% of the residue to be sea salt; corresponding measurements in the subtropics found a substantially lower sea salt fraction (25%). The contribution of sea salt to Br_y in the upper troposphere may be underestimated for at least two reasons. First, GEOS-Chem, and global models in general, do not consider the source of Br_y due to debromination of sea salt residue to the TTL. This Br_y source needs to be constrained and (if significant) incorporated into future global models. Second, GEOS-Chem driven with GEOS-5 meteorology underestimates the vertical transport in the tropics, as evidenced by MLS CO observations (42) and our comparison of O_3 profiles (Fig. 2*C*). Predictions of tropospheric O_3 profiles over the tEPO are sensitive to a choice of GEOS meteorological fields. We find good agreement between measured and predicted O_3 profiles with more vigorous tropical convective mass fluxes of GEOS-4 (available only until 2006; note that GEOS-5 predicts similar O_3 profiles between 2006 and 2012), which leads to lower O_3 over the tEPO, primarily because stronger convection dilutes stratospheric air with low O_3 air from the lower troposphere. We find that the model BrO distribution is largely insensitive to this increased convective mass flux (consistent with model treatment of Br_y washout as 100% effective). Br_y washout remains poorly understood, and stronger vertical transport emphasizes the need to better understand the efficiency of Br_y washout, which is likely a complex competition between the scavenging of soluble gases, the conversion rate of insoluble into soluble Br_y species by heterogeneous chemistry, and transport times into the FT.

Combined satellite (10) and balloon-borne measurements (25, 43) suggest the presence of ~8 pptv Br_y near the tropopause (14). Our observations find ~10 pptv Br_y in the lower TTL over the tEPO (*SI Appendix*, Fig. S6), where Br_y wet scavenging is thought to be effective (29, 31, 35). This inferred Br_y (*SI Appendix*, Fig. S6) is estimated using measured BrO and the box model calculated BrO/Br_y ratio (constrained by measurements; see *SI Appendix*). Very short-lived substances (including product gases) contribute 2–8 pptv Br_y to the stratosphere (34), in good agreement with the stratospheric boundary condition used in GEOS-Chem (31). The elevated BrO that we have measured in the SH LS corresponds to ~1.2 pptv ΔBr_y (Fig. 3*C*), which currently remains unexplained. The possible implications of a missing tropical inorganic bromine source for Br_y in the LS deserve further attention.

Atmospheric Implications

Halogen-Induced Tropospheric Ozone Loss. Halogen chemistry strongly affects the chemical lifetime of O_3 in the tropical troposphere. Over the tEPO, halogens account for 34% of the column-integrated tropospheric O_3 loss, and dominate the overall O_3 loss rates above 4 km (Fig. 4, error bars indicate atmospheric variability).

About 75% of the loss of tropospheric O_3 from halogen reactions occurs in the FT. Iodine destroys O_3 mostly below 3 km, while bromine destroys O_3 primarily at higher altitudes. Bromine accounts for 70% of the integral halogen-induced FT O_3 loss above 4 km. Above 12 km, ozone is destroyed at a rate of 0.6 ppb·d^{-1} mostly by bromine (71%) and iodine (15%); other reactions from HO_x (12%), photolysis (2%), and NO_y (<0.1%) are of minor importance. We note that BrO and IO chemistry are decoupled in the FT. The ozone loss rate due to bromine or iodine varies by ∼1% if the BrO + IO reactions is turned off in the model, suggesting that the reaction between BrO and IO does not add significantly to O_3 loss in the FT. This is primarily due to the much lower IO abundance in the FT compared with previous studies (1). Finally, *SI Appendix*, Fig. S8 projects the bromine-induced tropospheric ozone loss onto the global context. GEOS-Chem finds on average ∼2–7% total ozone loss due to bromine chemistry in the tropics, in agreement with previous studies (3); this is a lower limit compared with estimates that use observed BrO and IO. More vertically resolved measurements are needed to better constrain the global effect of halogen chemistry on tropospheric O_3 loss in other longitude and latitude ranges, and in different seasons.

Oxidation Capacity. By destroying O_3, halogens reduce an important primary source for OH radicals (*SI Appendix*, Fig. S9*A*). On the other hand, the reactions of IO + HO_2 and BrO + HO_2 effectively convert HO_2 into OH radicals (via photolysis of HOI and HOBr intermediates) (1, 2). However, the column-integrated secondary OH radical source is ∼7.7 times smaller than the recycling flux from the HO_2 + NO and HO_2 + O_3 reactions (combined, *SI Appendix*, Fig. S9*A*). At constant O_3, this secondary OH source from halogen chemistry leads to 4.1% higher OH (column integral in *SI Appendix*, Fig. S9*B*). We conclude that the effect of tropospheric bromine and iodine chemistry in reducing OH by destroying O_3 is ∼8 times larger than the secondary OH source. As a consequence, the net effect of halogen chemistry is to reduce OH radical concentrations, which leads to a lengthening in the CH_4 lifetime. Notably, a recent GEOS-Chem study found ∼4% lower OH radicals due to bromine chemistry (6), which is generally consistent with our above estimate of the combined effect of bromine and iodine. The effect of halogens in modifying OH and O_3 in the upper FT (*SI Appendix*, Fig. S9) is primarily driven by bromine chemistry. The representation of bromine chemistry in atmospheric models is currently poorly understood and deserves attention from the atmospheric chemistry and climate communities.

Climate Relevance. The current Intergovernmental Panel on Climate Change estimates of radiative forcing do not yet include the tropospheric chemistry of bromine and iodine. Br_y in the upper troposphere is highly sensitive to stratospheric Br_y that has increased since the preindustrial due to anthropogenic halon and CH_3Br emissions. Early studies have estimated a forcing from halogen-induced O_3 loss to be –0.1 W·m^{-2} (3). Our measurements suggest that naturally occurring halogen chemistry is more vigorous at destroying O_3 than is currently understood. Heterogeneous reactions involving O_3 are known to activate halogens from aerosol surfaces (36, 44), but these processes currently remain untested and might help explain some of the underestimated BrO. The hypothesis of an O_3 feedback to activate tropospheric halogen chemistry deserves further attention in light of increasing global background O_3 trends. Moreover, tropospheric bromine has been shown to help with the challenge faced by several global models to reproduce the low O_3 observed at the beginning of the 20th century (6). The more vigorous naturally occurring halogen chemistry likely helps to meet this challenge, which in turn would imply a stronger change in the radiative effect of tropospheric O_3 since preindustrial times than current forcing estimates (+0.4 W·m^{-2}) suggest (7).

Atmospheric Mercury Oxidation. It has been hypothesized that bromine may be the dominant oxidant that initiates the oxidation of atmospheric mercury (*SI Appendix*, Fig. S9) (45, 46). At the observed BrO concentrations, the lifetime of elemental mercury is only a few days in the upper tropical FT (*SI Appendix*, Fig. S9). Given the model underestimates of BrO, gaseous oxidized mercury, Hg(II), production is likely 2.8–3.5 times larger (column integral) than currently assumed (*SI Appendix*, Fig. S9). Our BrO measurements enable calculations of the rate of Hg(II) formation that are largely independent (<20% error) of uncertainty in the mercury oxidation mechanism (4, 6, 47), since the inferred bromine atom concentrations determine the rate limiting step for Hg(II) formation (5) (*SI Appendix*). We find that 83–91% of the tropospheric Hg(II) production occurs in the upper FT (8–14 km), consistent with observations that are thus far unexplained (48–50). Furthermore, the molecular identity of Hg(II) has not yet been determined, and the oxidation mechanism remains poorly understood. At the observed amounts of BrO, in the lower FT, the bromine reaction with mercury will be the dominant pathway to initialize mercury oxidation. The calculations further show that reactions of HO_2 and NO_2 with Hg –Br adducts (47) are relevant for the Hg(II) source and product distributions, and quantify their potential contributions over the full range of tropospheric altitudes. These reactions modify the Hg(II) source particularly in the lower FT (a factor of 20; *SI Appendix* and Fig. S10), where Hg(II) is more susceptible to dry (51) and wet deposition (52). Our study indicates that atmospheric mercury is a rather chemically dynamic component of air that warrants future study. Atmospheric deposition is the primary source of mercury to oceans (53), and the accurate representation of BrO profiles in atmospheric models is necessary for determining the global sources, speciation, distribution, and removal of Hg(II), with implications for public health concerns that arise from bioaccumulation of this neurotoxin in fish (53).

Methods

The TORERO project deployed a combination of chemical in situ and remote sensing instruments aboard the National Science Fountain/National Center for Atmospheric Research Gulfstream V aircraft (NSF/NCAR GV) to conduct a series of RFs over the EPO. Flights were based out of Antofagasta, Chile, and San Jose, Costa Rica. *SI Appendix*, Table S1 contains details on the presented case studies. BrO, IO, NO_2, H_2O, and O_4 were measured by the CU AMAX-DOAS (see below) instrument (19, 54); organohalogens ($CHBr_3$, CH_2Br_2, CH_2BrCl, $CHBr_2Cl$, CH_3I) and nonmethane hydrocarbons by the in situ TOGA (55); temperature profiles by the Microwave Temperature Profiler (56); and spectral actinic flux by the High-performance Instrumented Airborne Platform for Environmental Research Airborne Radiation Package. The photolysis frequencies were calculated from the actinic flux data using a modified version of the TUV model (Tropospheric Ultraviolet and Visible Radiation Model). Aerosol size distributions were measured by an ultra high sensitivity aerosol spectrometer and used to calculate aerosol surface area. Aerosol backscatter cross-section and depolarization measurements were obtained by a GV HSRL (57). O_3, CO, and H_2O (Vertical Cavity Surface Emitting Laser Hygrometer) (58) were measured by in situ sensors.

BrO and IO vertical profiles were measured by limb observations of scattered solar photons from CU AMAX-DOAS (Airborne Multi AXis Differential Optical Absorption Spectroscopy). Typical detection limits are ∼0.3–0.6 pptv BrO, ∼0.04 –0.1 pptv IO, ∼5–10 pptv NO_2, and ∼50–120 ppmv H_2O in the FT (19). We used the radiative transfer model McArtim (59), and demonstrate control over radiative transfer through comparison of remote sensing and in situ H_2O (see *SI Appendix*, Fig. S2), and O_4 (19). See Volkamer et al. (19) for more details. Note that 1 pptv = 1 part per trillion by volume ≈ 2.46 × 10^7 molecules per cubic centimeter (101,325 Pa, 298 K), and 1 ppmv = 10^3 ppbv = 10^6 pptv.

The Real-time Air Quality Modeling System was used for analysis of air mass origin and statistics on 7-d back-trajectories (see *SI Appendix*) (60). GEOS-Chem (v9.2, which includes bromine chemistry by default) is driven by GEOS-5 meteorological analyses, and was used for sensitivity studies on LS-Br_y and sensitivity studies of different meteorological fields (GEOS4), and to provide constraints about Br_y to the box model. Stratospheric concentrations (monthly and diurnally varying) of Br_y (Br, BrO, HOBr, HBr, $BrNO_3$, and Br_2) are taken from a GEOS-CCM (Goddard Chemistry Climate

Model) simulation (31). The ozone loss rate calculations, sensitivity studies of bromine sources, and mercury oxidation rates used an in-house-developed box model (20).

ACKNOWLEDGMENTS. We thank Paul Ziemann for proofreading the manuscript. The TORERO project is funded by the National Science Foundation (NSF) under Award AGS-1104104 (Principle Investigator: R.V.). The involvement of the NSF-sponsored Lower Atmospheric Observing Facilities, managed and operated by the National Center for Atmospheric Research Earth Observing Laboratory, is acknowledged. S.W. is a recipient of the Fulbright Junior Research Award; S.B. is a recipient of an Earth System Research Laboratory/Cooperative Institute for Research in Environmental Sciences graduate fellowship. R.V. acknowledges financial support from National Science Foundation Faculty Early Career Development Award ATM-0847793, Department of Energy Award DE-SC0006080, and Electric Power Research Institute Contracts EP-P27450/C13049 and EP-P32238/C14974 that supported the development of the AMAX-DOAS instrument and software/data analysis tools used in this study. D.J. is supported by NASA Atmospheric Chemistry Modeling and Analysis Program, and J.A.S. acknowledges support from The Danish Council for Independent Research | Natural Sciences.

1. Read KA, et al. (2008) Extensive halogen-mediated ozone destruction over the tropical Atlantic Ocean. *Nature* 453(7199):1232–1235.
2. von Glasow R, von Kuhlmann R, Lawrence M, Platt U, Crutzen P (2004) Impact of reactive bromine chemistry in the troposphere. *Atmos Chem Phys* 4(11/12):2481–2497.
3. Saiz-Lopez A, et al. (2012) Estimating the climate significance of halogen-driven ozone loss in the tropical marine troposphere. *Atmos Chem Phys* 12(9):3939–3949.
4. Holmes CD, Jacob DJ, Mason RP, Jaffe DA (2009) Sources and deposition of reactive gaseous mercury in the marine atmosphere. *Atmos Environ* 43(14):2278–2285.
5. Hynes A, Donohoue D, Goodsite M, Hedgecock I (2009) Our current understanding of major chemical and physical processes affecting mercury dynamics in the atmosphere and at the air-water/terrestrial interfaces. *Mercury Fate and Transport in the Global Atmosphere*, eds Mason R, Pirrone N (Springer, New York), pp 427–457.
6. Parrella J, et al. (2012) Tropospheric bromine chemistry: Implications for present and pre-industrial ozone and mercury. *Atmos Chem Phys* 12(15):6723–6740.
7. Intergovernmental Panel on Climate Change (2013) *Climate Change 2013: The Physical and Scientific Basis. Contribution to the IPCC Fifth Assessment Report* (Intergov Panel Clim Change, Stockholm).
8. Lelieveld J, Crutzen PJ, Dentener FJ (1998) Changing concentration, lifetime and climate forcing of atmospheric methane. *Tellus B Chem Phys Meterol* 50(2):128–150.
9. Mickley L, Jacob D, Field B, Rind D (2004) Climate response to the increase in tropospheric ozone since preindustrial times: A comparison between ozone and equivalent CO_2 forcings. *J Geophys Res* 109(D5):D05106.
10. Chance K (1998) Analysis of BrO measurements from the Global Ozone Monitoring Experiment. *Geophys Res Lett* 25(17):3335–3338.
11. Fitzenberger R, et al. (2000) First profile measurements of tropospheric BrO. *Geophys Res Lett* 27(18):2921–2924.
12. Wagner T, Leue C, Wenig M, Pfeilsticker K, Platt U (2001) Spatial and temporal distribution of enhanced boundary layer BrO concentrations measured by the GOME instrument aboard ERS-2. *J Geophys Res* 106(D20):24225–24235.
13. Richter A, Wittrock F, Ladstätter-Weißenmayer A, Burrows J (2002) GOME measurements of stratospheric and tropospheric BrO. *Adv Space Res* 29(11):1667–1672.
14. Salawitch RJ, et al. (2005) Sensitivity of ozone to bromine in the lower stratosphere. *Geophys Res Lett* 32(5):811–816.
15. Hendrick F, et al. (2007) Retrieval of stratospheric and tropospheric BrO profiles and columns using ground-based zenith-sky DOAS observations at Harestua, 60°N. *Atmos Chem Phys* 7(18):4869–4885.
16. Theys N, et al. (2007) Retrieval of stratospheric and tropospheric BrO columns from multi-axis DOAS measurements at Reunion Island (21°S, 56°E). *Atmos Chem Phys* 7(18):4733–4749.
17. Coburn S, Dix B, Sinreich R, Volkamer R (2011) The CU ground MAX-DOAS instrument: Characterization of RMS noise limitations and first measurements near Pensacola, FL of BrO, IO, and CHOCHO. *Atmos Meas Tech* 4(11):2421–2439.
18. Theys N, et al. (2011) Global observations of tropospheric BrO columns using GOME-2 satellite data. *Atmos Chem Phys* 11(4):1791–1811.
19. Volkamer R, et al. (2015) Aircraft measurements of BrO, IO, glyoxal, NO_2, H_2O, O_2–O_2 and aerosol extinction profiles in the tropics: Comparison with aircraft-/ship-based in situ and lidar measurements. *Atmos Meas Tech* 8(5):2121–2148.
20. Dix B, et al. (2013) Detection of iodine monoxide in the tropical free troposphere. *Proc Natl Acad Sci USA* 110(6):2035–2040.
21. Puentedura O, et al. (2012) Iodine monoxide in the north subtropical free troposphere. *Atmos Chem Phys* 12(11):4909–4921.
22. Carslaw KS, et al. (2013) Large contribution of natural aerosols to uncertainty in indirect forcing. *Nature* 503(7474):67–71.
23. Nowack PJ, et al. (2015) A large ozone-circulation feedback and its implications for global warming assessments. *Nat Clim Change* 5(January):41–45.
24. Dorf M, et al. (2008) Bromine in the tropical troposphere and stratosphere as derived from balloon-borne BrO observations. *Atmos Chem Phys* 8(23):7265–7271.
25. Pundt I, Pommereau J-P, Chipperfield M, Van Roozendael M, Goutail F (2002) Climatology of the stratospheric BrO vertical distribution by balloon-borne UV–visible spectrometry. *J Geophys Res* 107(D24):4806.
26. Carpenter LJ, et al. (2013) Atmospheric iodine levels influenced by sea surface emissions of inorganic iodine. *Nat Geosci* 6(2):108–111.
27. Yang X, et al. (2005) Tropospheric bromine chemistry and its impacts on ozone: A model study. *J Geophys Res* 110(D23):D23311.
28. Sander R, et al. (2003) Inorganic bromine in the marine boundary layer: A critical review. *Atmos Chem Phys* 3(5):1301–1336.
29. Fernandez R, Salawitch R, Kinnison D, Lamarque J-F, Saiz-Lopez A (2014) Bromine partitioning in the tropical tropopause layer: Implications for stratospheric injection. *Atmos Chem Phys* 14(24):13391–13410.
30. Long MS, et al. (2014) Sensitivity of tropospheric chemical composition to halogen-radical chemistry using a fully coupled size-resolved multiphase chemistry–global climate system: Halogen distributions, aerosol composition, and sensitivity of climate-relevant gases. *Atmos Chem Phys* 14(7):3397–3425.
31. Liang Q, et al. (2014) Convective transport of very short lived bromocarbons to the stratosphere. *Atmos Chem Phys* 14(11):5781–5792.
32. Waugh DW, Polvani LM (2000) Climatology of intrusions into the tropical upper troposphere. *Geophys Res Lett* 27(23):3857–3860.
33. Munchak LA, Pan LL (2014) Separation of the lapse rate and the cold point tropopauses in the tropics and the resulting impact on cloud top-tropopause relationships. *J Geophys Res Atmos* 119(13):7963–7978.
34. World Meteorological Organization (2014) *Scientific Assessment of Ozone Depletion: 2014* (World Meteorol Org, Geneva).
35. Aschmann J, Sinnhuber BM, Chipperfield MP, Hossaini R (2011) Impact of deep convection and dehydration on bromine loading in the upper troposphere and lower stratosphere. *Atmos Chem Phys* 11(6):2671–2687.
36. Ammann M, et al. (2013) Evaluated kinetic and photochemical data for atmospheric chemistry: Volume VI – heterogeneous reactions with liquid substrates. *Atmos Chem Phys* 13(16):8045–8228.
37. Lee M-T, et al. (2014) Competition between organics and bromide at the aqueous solution–air interface as seen from ozone uptake kinetics and X-ray photoelectron spectroscopy. *J Phys Chem A* 119(9):4600–4608.
38. Roberts TJ, Jourdain L, Griffiths PT, Pirre M (2014) Re-evaluating the reactive uptake of HOBr in the troposphere with implications for the marine boundary layer and volcanic plumes. *Atmos Chem Phys* 14(20):11185–11199.
39. Sassen K, Wang Z, Liu D (2009) Cirrus clouds and deep convection in the tropics: Insights from CALIPSO and CloudSat. *J Geophys Res* 114(D4):D00H06.
40. Froyd KD, Murphy DM, Lawson P, Baumgardner D, Herman RL (2010) Aerosols that form subvisible cirrus at the tropical tropopause. *Atmos Chem Phys* 10(1):209–218.
41. Cziczo DJ, et al. (2013) Clarifying the dominant sources and mechanisms of cirrus cloud formation. *Science* 340(6138):1320–1324.
42. Liu J, et al. (2012) Transport analysis and source attribution of seasonal and interannual variability of CO in the tropical upper troposphere and lower stratosphere. *Atmos Chem Phys Discuss* 12(7):17397–17442.
43. Wamsley PR, et al. (1998) Distribution of halon-1211 in the upper troposphere and lower stratosphere and the 1994 total bromine budget. *J Geophys Res* 103(D1):1513–1526.
44. Sander SP, et al. (2011) *Chemical Kinetics and Photochemical Data for Use in Atmospheric Studies, Evaluation No. 17* (Jet Propulsion Laboratory, Pasadena, CA), *Publ 10-6*.
45. Holmes CD, Jacob DJ, Yang X (2006) Global lifetime of elemental mercury against oxidation by atomic bromine in the free troposphere. *Geophys Res Lett* 33(20):L20808.
46. Holmes CD, et al. (2010) Global atmospheric model for mercury including oxidation by bromine atoms. *Atmos Chem Phys* 10(24):12037–12057.
47. Dibble T, Zelie M, Mao H (2012) Thermodynamics of reactions of ClHg and BrHg radicals with atmospherically abundant free radicals. *Atmos Chem Phys* 12(21):10271–10279.
48. Lyman SN, Jaffe DA (2011) Formation and fate of oxidized mercury in the upper troposphere and lower stratosphere. *Nat Geosci* 5(2):114–117.
49. Murphy DM, Hudson PK, Thomson D, Sheridan PJ, Wilson JC (2006) Observations of mercury-containing aerosols. *Environ Sci Technol* 40(10):3163–3167.
50. Talbot R, Mao H, Scheuer E, Dibb J, Avery M (2007) Total depletion of Hg in the upper troposphere–lower stratosphere. *Geophys Res Lett* 34(23):L23804.
51. Weiss-Penzias P, Gustin MS, Lyman SN (2009) Observations of speciated atmospheric mercury at three sites in Nevada: Evidence for a free tropospheric source of reactive gaseous mercury. *J Geophys Res* 114(D14):D14302.
52. Nair US, et al. (2013) Cloud-resolving simulations of mercury scavenging and deposition in thunderstorms. *Atmos Chem Phys* 13:10143–10157.
53. Selin NE (2009) Global biogeochemical cycling of mercury: A review. *Annu Rev Environ Resour* 34(1):43–63.
54. Baidar S, et al. (2013) The CU Airborne MAX-DOAS instrument: Vertical profiling of aerosol extinction and trace gases. *Atmos Meas Tech* 6(3):719–739.
55. Apel EC, et al. (2010) Chemical evolution of volatile organic compounds in the outflow of the Mexico City metropolitan area. *Atmos Chem Phys* 10(5):2353–2375.
56. Lim B, Mahoney MJ, Haggerty J, Denning R (2013) The microwave temperature profiler performance in recent airborne campaigns. *IEEE Int Geosci Remote Sens Symp*. 2013: 3363–3366.
57. Eloranta E, Razenkov I, Hedrick J, Garcia J (2008) The design and construction of an airborne High Spectral Resolution Lidar. *IEEE Aerospace Conf* 2008:1–6.
58. Zondlo MA, Paige ME, Massick SM, Silver JA (2010) Vertical cavity laser hygrometer for the National Science Foundation Gulfstream-V aircraft. *J Geophys Res* 115(D20):D20309.
59. Deutschmann T, et al. (2011) The Monte Carlo atmospheric radiative transfer model McArtim: Introduction and validation of Jacobians and 3D features. *J Quant Spectrosc Radiat Transfer* 112(6):1119–1137.
60. Pierce RB, et al. (2007) Chemical data assimilation estimates of continental US ozone and nitrogen budgets during the Intercontinental Chemical Transport Experiment–North America. *J Geophys Res* 112(D12):D12S21.